Desalination and Water Treatment
www.deswater.com
doi: 10.5004/dwt.2022.28368

256 (2022) 35–50
April

Optimization of APTES/TiO_2 nanomaterials modification conditions for antibacterial properties and photocatalytic activity

Agnieszka Sienkiewicz, Paulina Rokicka-Konieczna*, Agnieszka Wanag, Ewelina Kusiak-Nejman, Antoni W. Morawski

Department of Inorganic Chemical Technology and Environment Engineering, Faculty of Chemical Technology and Engineering, West Pomeranian University of Technology in Szczecin, Pułaskiego 10, 70-322 Szczecin, Poland, emails: Paulina.Rokicka@zut.edu.pl (P. Rokicka-Konieczna), Agnieszka.Sienkiewicz@zut.edu.pl (A. Sienkiewicz), Agnieszka.Wanag@zut.edu.pl (A. Wanag), Ewelina.Kusiak@zut.edu.pl (E. Kusiak-Nejman), Antoni.Morawski@zut.edu.pl (A.W. Morawski)

Received 7 September 2021; Accepted 8 March 2022

ABSTRACT

In this work, the influence of the modifier concentration and the temperature of modification on the antibacterial and photocatalytic properties of titanium dioxide (TiO_2) functionalized with 3-aminopropyltriethoxysilane (APTES) was investigated. The new APTES/TiO_2 nanomaterials were obtained by the solvothermal method. The studies confirmed the presence of N, C and Si in the TiO_2 structure, indicating that the modification was performed successfully. Furthermore, the antibacterial properties of the samples were investigated based on *Escherichia coli* inactivation in saline solution. The decomposition of methylene blue determined the photocatalytic activity under UV irradiation. For the *E. coli* inactivation process, the best concentration of the photocatalyst was 0.1 g/L, while for dye degradation tests, the optimum semiconductor dose was 0.5 g/L. The best antibacterial properties presented photocatalysts obtained by modification with 250 mM of APTES solution. In the case of methylene blue decomposition, the photoactivity increased with the increase of APTES concentration, while the modification temperature from 120°C to 180°C had no significant impact on the activity of the tested samples.

Keywords: Photocatalysis; Titanium dioxide; 3-aminopropyltriethoxysilane; Methylene blue; *Escherichia coli*

1. Introduction

The world is facing a major challenge: providing safe and clean drinking water. Therefore, water security is considered the overarching goal of water management [1]. However, numerous places in the world are still struggling to solve problems of water contaminated by biological and chemical compounds. For example, pathogenic bacteria like *Escherichia coli* are responsible for many diseases (e.g., diarrhoea, urethritis or bladder infection) and even human death [2,3]. In addition, many water bodies are contaminated with chemical pollutants, including organic dyes, which are one of the primary contaminants of industrial wastewater [4,5]. Therefore, the important challenge is to develop alternative methods of water purification and disinfection that are effective against a wide range of contaminants (both microbial and chemical).

According to Ismail et al. [4], a method based on nanotechnology (e.g., photocatalysis) is an excellent alternative to conventional water treatment techniques. In the available literature, there are many reports which confirm the high disinfectant effect of various photocatalysts (like WO_3, ZnO, SnO_2, $BiVO_4$, TiO_2) against bacteria [6–9]. Bekkali et al. [7], for example, obtained ZnO/hydroxyapatite nanomaterials

* Corresponding author.

which presented good antibacterial properties against *E. coli*, *Pseudomonas aeruginosa*, *Staphylococcus aureus* and *Enterococcus faecalis*. Gnanamoorthy et al. [8] synthesized SnO_2 nanorods, which showed good antibacterial activity against *Staphylococcus aureus*, *E. coli* and *Pseudomonas aeruginosa*. In turn, Sharma et al. [9] observed satisfactory biocidal properties of monoclinic bismuth vanadate (m-$BiVO_4$) nanostructures toward *E. coli*. Numerous studies have also confirmed excellent antibacterial properties of TiO_2 based nanomaterials [10,11]. TiO_2 is considered the most widely applied oxide in photocatalysis, and its biocidal properties have been demonstrated on a wide range of bacteria [12–14]. Unfortunately, TiO_2 presents also some limitations like rapid recombination of photogenerated electron–hole pairs. Consequently, one of the widely investigated subjects in photocatalysis is a modification of pure TiO_2 to overcome the mentioned problem. To improve the photocatalytic process efficiency, many different ways of TiO_2 modification are applied (e.g., surface modification or co-modification, dye sensitization, combining TiO_2 with other semiconductors) [15,16]. One method involves using organosilanes such as 3-aminopropyltriethoxysilane (APTES) for TiO_2 surface modification [17]. Silica modification can improve TiO_2 photocatalytic activity, among others, by decreasing particles size, enhancing the specific surface area, or repressing the phase transformation from anatase to rutile [18,19]. Our previous study also confirmed that APTES modification enhanced adsorption properties and photocatalytic activity of obtained TiO_2 nanomaterials [20].

In our previous reports, the impact of APTES/TiO_2 nanomaterials obtained by utilizing different concentrations of APTES on antibacterial properties [21] or methylene blue decomposition were examined [22]. In the present work, modification of TiO_2 with APTES was also performed. The research idea was to determine an optimal dose of modifier (APTES) related to photocatalytic activity. However, the simultaneous effect of the two parameters: APTES concentration and modification temperature on the photocatalytic inactivation of bacteria *E. coli* and methylene blue degradation was investigated for the first time. In addition, in this paper, optimization towards the appropriate dose of APTES/TiO_2 photocatalyst, necessary to determine both antibacterial properties and yield of dye decomposition, was presented for the first time. Moreover, it was decided to evaluate the effect of low-temperature modification in the range of 120°C–180°C on the photoefficiency of the prepared nanomaterials.

2. Experimental

2.1. Materials and reagents

Crude TiO_2 slurry prepared by sulfate technology, supplied from the chemical plant Grupa Azoty Zakłady Chemiczne "Police" S.A. (Poland), was selected as a TiO_2 source. Before modification, the raw TiO_2 was rinsed with an aqueous solution of NH_4OH (purity 25%, Firma Chempur®, Poland) to remove sulphuric compounds' residues forming ammonium sulfate that is easily soluble in water [22]. In the next step, the suspension was rinsed with distilled water until pH equalled 6.8. The prepared material was named starting-TiO_2. 3-aminopropyltriethoxysilane (APTES, purity ≥98%) purchased from Merck KGaA (Germany) was utilized as a modifier of TiO_2. Ethyl alcohol (purity 96%) from P.P.H. "STANLAB" Sp.J., (Poland) was selected as a solvent of APTES. *E. coli* K12 (ATCC 29425, LGC Ltd., USA) was selected as model microbial contamination of water. Methylene blue (purity ≥82%, Firma Chempur®, Poland) was chosen as a model organic water pollutant.

2.2. APTES/TiO_2 nanomaterials preparation technique

The APTES-modified TiO_2 photocatalysts were prepared by the solvothermal method. The modifier concentrations in ethanol were 50, 250, 450, and 650 mM. At first, 5 g of starting-TiO_2 was dispersed in 25 mL of APTES solution. Next, a sample was modified in a pressure autoclave for 4 h at 120°C, 140°C, 160°C and 180°C with provided continuous stirring at 500 rpm. Afterwards, the obtained suspension was rinsed with ethanol and distilled water to remove any residual chemicals. Finally, the prepared material was dried for 24 h at 105°C in a lab dryer. The gained photocatalysts were denoted as TiO_2-4h-X°C-YmM, where *X* is the modification temperature, and *Y* is the concentration of APTES in ethanol.

2.3. Characterization

The X-ray powder diffraction analysis (Melvern PANalytical B.V., Netherlands) using Cu Kα radiation (λ = 1.54056 Å) was used to identify the crystalline structure of the examined samples. To calculate the mean crystallites size, Scherrer's equation was used. The PDF-4+ 2014 International Centre for Diffraction Data database (04-005-5923 PDF4+ card for rutile and 04-002-8296 PDF4+ card for anatase) was applied to identify the phase composition. In order to calculate the Brunauer–Emmett–Teller (BET) specific surface area and pore volume, the low-temperature N_2 adsorption–desorption measurements, carried out at 77 K, were performed with the QUADRASORB evoTM Gas Sorption analyzer (Anton Paar GmbH, Austria). Before each measurement, all materials were degassed under a high vacuum for 12 h at 100°C to eliminate any remaining impurities on the examined samples' surface. The total pore volume (V_{total}) was determined by the single point from the nitrogen adsorption isotherms at relative pressure p/p_0 = 0.99. The Dubinin–Radushkevich method was used to estimate the volume of micropores (V_{micro}), while the volume of mesopores (V_{meso}) was calculated as the difference between V_{total} and V_{micro}. The Fourier-transform infrared spectroscopy (FT-IR) 4200 spectrometer (JASCO International Co. Ltd., Japan) supplied with DiffuseIR accessory (PIKE Technologies, USA) was applied to identify the surface functional groups of APTES/TiO_2 nanomaterials. The ZetaSizer NanoSeries ZS (Malvern PANalytical Ltd., UK) was used to measure the zeta potential values. A CN628 elemental analyzer (LECO Corporation, USA) was used to determine total carbon and nitrogen content in tested samples. To prepare the calibration curve, a certified ethylenediaminetetraacetic acid (EDTA) standard (Elemental Microanalysis Ltd., UK), containing 41.04 ± 0.15 wt.% carbon and 9.56 ± 0.11 wt.% nitrogen was utilized. The surface morphology of the APTES/TiO_2 photocatalysts was observed via scanning electron microscopy (SEM) using a Hitachi SU8020 ultra-high resolution field emission

scanning electron microscope (Hitachi Ltd., Japan). The energy-dispersive X-ray spectroscopy (EDX) from Thermo Fisher Scientific Inc. (USA) was used to perform EDX mapping analysis of the tested samples.

The analysis of hydroxyl radical formation on photocatalysts surface was determined by fluorescence technique using terephthalic acid (Acros Organics B.V.B.A, Belgium). The fluorescence product of terephthalic acid hydroxylation, 2-hydroxyterephthalic acid (2-HTA), was detected as an emission peak at the maximum wavelength of 420 nm, with the 314 nm excitation wavelength and analysed on a Hitachi F-2500 fluorescence spectrophotometer (Hitachi Ltd., Japan).

2.4. Light source

Both antibacterial tests and photocatalytic activity studies were conducted under UV-Vis light with the radiation intensity of 65 W/m^2 for 300–2800 nm and 36 W/m^2 for the 280–400 nm region, provided by 6 lamps of 20 W each (Philips, Amsterdam, Netherlands). The radiation source used was called UV light due to the low intensity of visible radiation.

2.5. Antibacterial tests

The antibacterial properties of photocatalysts were determined using the standard plate count method toward the gram-negative *E. coli* K12 (ATCC 29425, LGC Ltd, USA). Before the experiments, bacteria were inoculated into Enriched Broth (BioMaxima S.A., Poland) and cultured at 37°C for 24 h. Next, bacteria were harvested through centrifugation (4,000 rpm, 10 min) and then re-suspended in sterile saline solution (0.9% NaCl, Firma Chempur®, Poland). The concentration of the bacteria was adjusted to approx. 1.5×10^7 CFU/mL by optical density measurement at a wavelength of 600 nm.

The antibacterial experiments were carried out in a sterilized 150 ml glass beaker containing 90 mL of saline solution, 10 mL of the bacterial suspension (1.5×10^7 CFU/mL) and appropriate photocatalyst (in a concentration of 0.05, 0.1, 0.25, 0.5 or 0.75 g/L). The suspension was continuously stirred to ensure homogeneity and irradiated with UV light for 90 min at room temperature. The distance between the reactor and the light source was fixed at approx. 35 cm. At given time intervals, 1 ml of bacterial suspension was collected and diluted by decimal dilution method in saline solution. Next, suspensions were spread on the Petri dish containing Plate Count Agar (BioMaxima S.A., Poland) and incubated at 37°C for 24 h. After incubation, the number of viable colonies was counted and depicted as log CFU/mL. Control experiments (under the dark conditions and for the saline solution) were also conducted. All measurements were performed in triplicates. The standard error of the measurements amounted less than 10%.

2.6. Photocatalytic activity studies

Before the photocatalytic activity studies, adsorption measurements were performed. A 0.6 L glass beaker containing 0.5 L of methylene blue solution with an initial concentration of 15 mg/L and 0.05, 0.1, 0.25, 0.5 or 0.75 g/L of the appropriate photocatalyst was placed in a thermostatic chamber at 20°C (Pol-Eko-Aparatura sp.j., Poland) in light-free conditions and stirred for 60 min to provide the adsorption–desorption equilibrium between dye molecules and the surface of the tested sample. After that, the solution was irradiated with UV light. The methylene blue concentration was analyzed every 60 min during photoactivity tests by the V-630 UV-Vis spectrometer (JASCO International Co., Japan). Before each measurement, 10 mL of the taken suspension was centrifuged to eliminate all suspended nanoparticles. Methylene blue decomposition degree was calculated based on the equation:

$$R\left[\%\right] = \frac{C_0 - C_t}{C_t} \times 100\% \quad (1)$$

where R is methylene blue decomposition degree (%), C_0 is the initial concentration of methylene blue measured after adsorption (mg/L), and C_t is the methylene blue concentration at the time t (mg/L).

3. Results and discussion

3.1. Characterization of the nanomaterials

3.1.1. X-ray powder diffraction analysis

X-ray diffraction (XRD) patterns of starting-TiO_2 and APTES-modified TiO_2 photocatalysts are shown in Fig. 1A–D. All nanomaterials exhibited reflections characteristic for anatase phase located at 25.3°, 37.8°, 48.1°, 53.9°, 55.1°, 62.7°, 68.9°, 70.3° and 75.1°, and some reflections characteristic for rutile phase: located at 27.4°, 36.0° and 41.2° [20]. The presence of rutile in the starting-TiO_2 is due to the addition of rutile nuclei during the manufacturing process of crude TiO_2 pulp via the sulfate method. According to the data presented in Table 1, all photocatalysts consist mainly of the anatase phase (94%–96%) with a small amount of a rutile phase (4–6%). Moreover, modification in the temperature range from 120°C to 180°C did not cause the anatase-to-rutile phase transformation, which is typical because anatase transforms into a rutile phase above 600°C [23]. Additionally, no significant changes in the crystalline structure of the tested samples were noted, which was consistent with the results obtained by Klaysri et al. [17]. They observed that the surface functionalization with APTES in the concentration range of 0.1–100 mM did not influence the phase structure and the crystalline size of titanium dioxide, which were about 17–19 nm, where in our case the crystallite size of anatase was in the range of 14 to 16 nm and rutile from 21 to 62 nm. Due to the low content of the rutile phase (4%–6%), the noted changes in the rutile crystallites size may have resulted from the conversion error of the method.

3.1.2. FT-IR/DRS (differential reflectance spectroscopy) measurements

All FT-IR/differential reflectance spectroscopy (DRS) (Fig. 2A–D) were characterized by a narrow band at around 1,628 cm^{-1} and a wide band from 3,750 to 2,500 cm^{-1}, ascribed to the molecular water and stretching mode of surface –OH groups, respectively [24,25]. On the spectra of the modified photocatalysts, characteristic bands originating

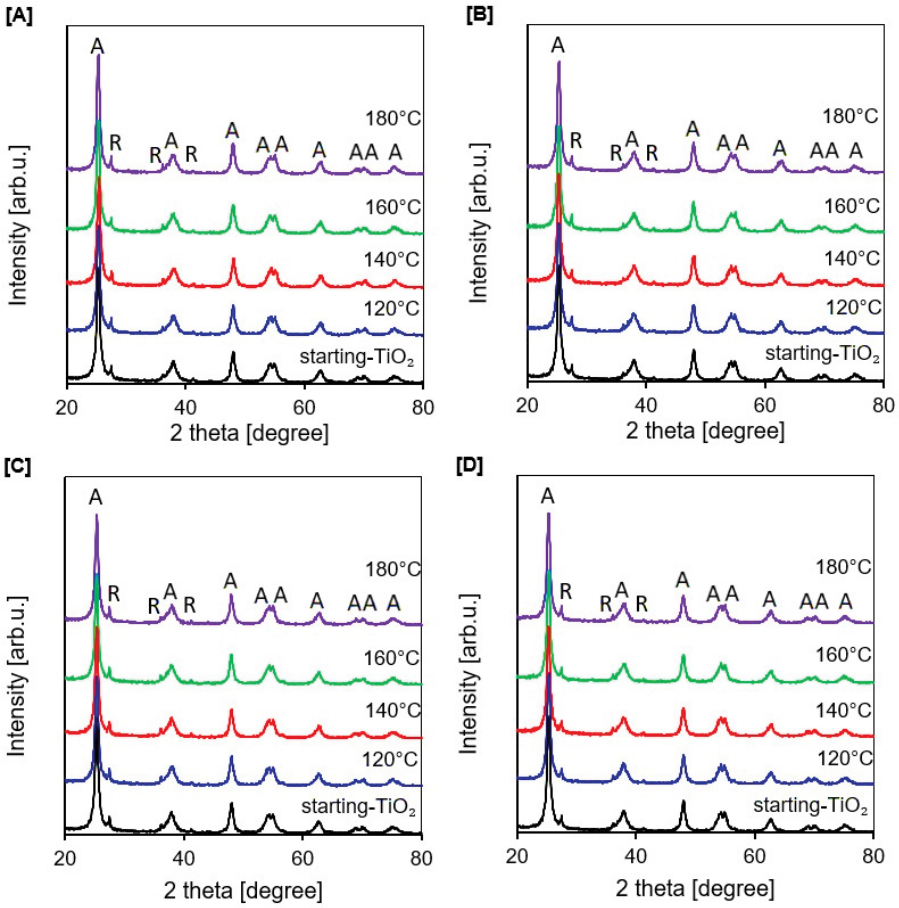

Fig. 1. X-ray diffraction (XRD) patterns of starting-TiO_2 and TiO_2 nanomaterials modified with APTES concentration of 50 mM (A), 250 mM (B), 450 mM (C), and 650 mM (D), where A-anatase, R-rutile.

Table 1
Physico-chemical properties of starting-TiO_2 and APTES-modified TiO_2 nanomaterials

Sample name	S_{BET} (m^2/g)	V_{total} (cm^3/g)	V_{micro} (cm^3/g)	V_{meso} (cm^3/g)	Anatase in crystallite phase (%)	Anatase crystallite size (nm)	Rutile in crystallite phase (%)	Rutile crystallite size (nm)
Starting-TiO_2	207	0.370	0.070	0.300	95	14	5	21
TiO_2-4h-120°C-50mM	185	0.280	0.070	0.210	95	15	5	40
TiO_2-4h-140°C-50mM	194	0.380	0.068	0.312	95	15	5	54
TiO_2-4h-160°C-50mM	189	0.386	0.066	0.320	94	15	6	27
TiO_2-4h-180°C-50mM	188	0.358	0.060	0.298	96	16	4	48
TiO_2-4h-120°C-250mM	148	0.290	0.060	0.230	95	15	5	56
TiO_2-4h-140°C-250mM	144	0.298	0.052	0.246	95	15	5	48
TiO_2-4h-160°C-250mM	150	0.304	0.054	0.249	95	15	5	48
TiO_2-4h-180°C-250mM	135	0.223	0.051	0.172	96	15	4	37
TiO_2-4h-120°C-450mM	133	0.195	0.051	0.140	95	15	5	31
TiO_2-4h-140°C-450mM	137	0.232	0.052	0.180	95	15	5	36
TiO_2-4h-160°C-450mM	137	0.226	0.052	0.174	96	15	4	48
TiO_2-4h-180°C-450mM	133	0.216	0.050	0.166	95	14	5	62
TiO_2-4h-120°C-650mM	128	0.199	0.050	0.149	96	15	4	39
TiO_2-4h-140°C-650mM	125	0.279	0.047	0.232	96	15	4	36
TiO_2-4h-160°C-650mM	131	0.218	0.049	0.159	96	15	4	45
TiO_2-4h-180°C-650mM	135	0.281	0.049	0.232	96	15	4	41

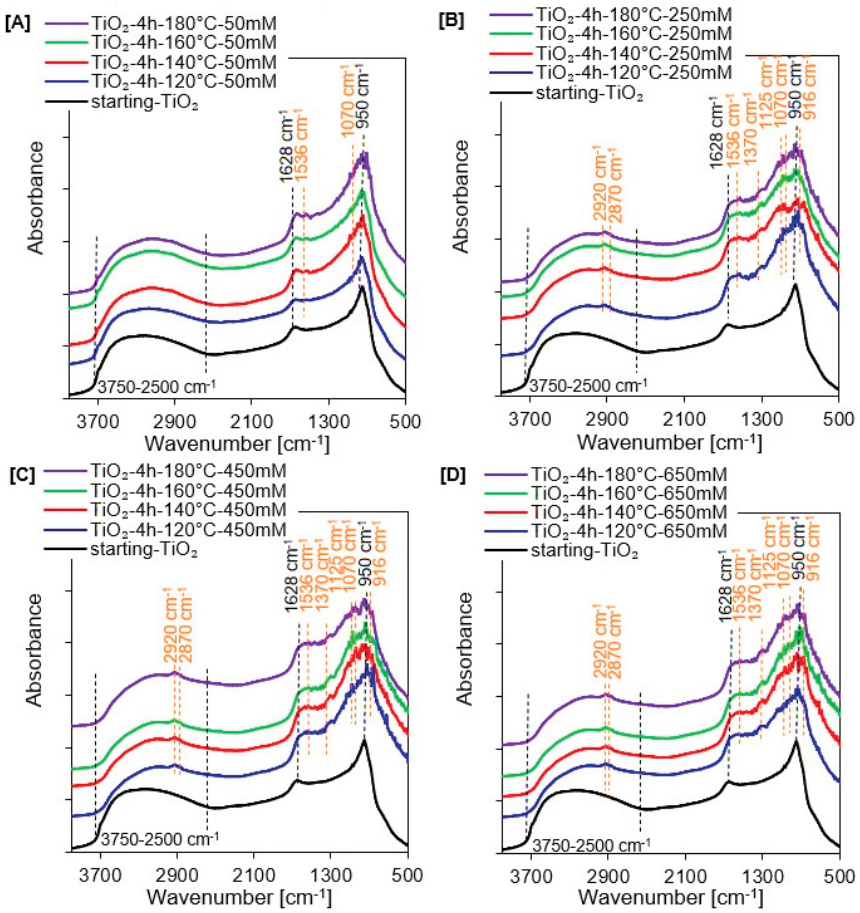

Fig. 2. FT-IR/DR spectra of starting-TiO_2 and TiO_2 nanomaterials modified with APTES concentration of 50 mM (A), 250 mM (B), 450 mM (C), and 650 mM (D).

from APTES were observed, which indicates that APTES/TiO_2 nanomaterials were prepared successfully. As the modification temperature increased, there were no significant changes in the surface characteristics of the tested materials. However, the amount and intensity of bands characteristic for APTES increased with increasing modifier concentration. In Fig. 2A, showing spectra of samples functionalized with 50 mM of APTES, the scissor vibrations of primary amine groups at around 1,536 cm^{-1} and Si–O–C groups at around 1,070 cm^{-1} were noted [26,27]. In Fig. 2B–D, additional bands typical for APTES were also noted – the bending and stretching modes of the alkyl groups detected at 2,929 and 2,879 cm^{-1} [27,28]. Bands at 1,370 and 1,125 cm^{-1} correspond to the symmetric C–H bending modes and asymmetric stretching vibrations of Si–O–Si, respectively [27,29–31]. Bands observed in the range from 960 to 910 cm^{-1} are attributed to the stretching vibrations of Ti–O–Si bonds. Moreover, the bond at around 916 cm^{-1} indicates that the condensation between surface hydroxyl groups and silanol groups occurred [32,33].

3.1.3. BET specific surface area and pore volume analysis

According to Fig. S1A–D, the adsorption–desorption isotherms of all tested photocatalysts based on the IUPAC classification, showed a type IV nitrogen isotherm. Typical features of this type of isotherm are its hysteresis loop, associated with capillary condensation occurring in mesopores, and the limitation of uptake in the range of high p/p_0 values [34]. Moreover, these nanomaterials presented the same H_3 type of hysteresis loop which is marked by slit-shaped pores and often continue into the low-pressure region [35,36]. It is worth mentioning that the size of the hysteresis loops presented in Fig. S1A–D decreased with increasing APTES concentration related to the decreasing amount of mesopores in the materials (Table 1) [37]. However, there was no significant effect of the modification temperature between 120°C and 180°C on the change in the size of the hysteresis loops. Thus no significant effect on the change of the specific surface area and total pore volume of the tested samples was noted. The specific surface area for starting-TiO_2 was 207 m^2/g, while APTES/TiO_2 nanomaterials ranged from 194 to 125 m^2/g. Furthermore, based on the data listed in Table 1, it was found that the decrease not only of S_{BET} but also of V_{total}, V_{meso} and a slight decrease of V_{micro} with increasing APTES concentration suggests that modifier molecules are not only placed on the TiO_2 outer surface but also captured in the pores. A similar effect was observed by Dalod et al. [28], Ukaji et al. [32], Zhuang et al. [38] and Pontón et al. [39].

Table 2
The zeta potential values and carbon and nitrogen content of starting-TiO_2 and APTES-modified TiO_2 nanomaterials

Sample name	Zeta potential δ (mV)	Carbon content (wt.%)	Nitrogen content (wt.%)
Starting-TiO_2	+12.80	–	0.18
TiO_2-4h-120°C-50mM	+15.75	1.16	0.43
TiO_2-4h-140°C-50mM	+13.83	1.14	0.44
TiO_2-4h-160°C-50mM	+15.02	1.17	0.43
TiO_2-4h-180°C-50mM	+15.70	1.25	0.44
TiO_2-4h-120°C-250mM	+17.89	3.22	1.13
TiO_2-4h-140°C-250mM	+20.26	3.49	1.24
TiO_2-4h-160°C-250mM	+21.96	3.53	1.25
TiO_2-4h-180°C-250mM	+22.34	3.64	1.27
TiO_2-4h-120°C-450mM	+23.12	3.76	1.32
TiO_2-4h-140°C-450mM	+25.53	3.70	1.28
TiO_2-4h-160°C-450mM	+26.18	3.72	1.31
TiO_2-4h-180°C-450mM	+26.73	3.87	1.35
TiO_2-4h-120°C-650mM	+26.18	3.34	1.30
TiO_2-4h-140°C-650mM	+24.90	4.10	1.39
TiO_2-4h-160°C-650mM	+27.11	3.98	1.31
TiO_2-4h-180°C-650mM	+26.95	4.15	1.76

3.1.4. Zeta potential analysis

Based on the data presented in Table 2, all photocatalysts were characterized by positive surface charge, and the zeta potential values changed from +12.80 mV for starting-TiO_2 to +27.11 mV for TiO_2-4h-160°C-650 mM sample. According to Talavera-Pech et al. [40], Youssef et al. [41], and Zhao et al. [42], APTES has cationic amino groups, which can easily bond to the semiconductor surface. Thus, the zeta potential values of the amino-functionalized TiO_2 nanomaterials enhanced with increasing concentration of APTES used for the modification, which was due to the higher presence of $–NH_2$ groups on the surface of the obtained samples. The presence of the positively charged amino groups on the TiO_2 surface was confirmed by FT-IR/DRS measurements and the nitrogen content analysis shown in Fig. 2A–D and Table 2, respectively.

3.1.5. Carbon and nitrogen content analysis

According to the results presented in Table 2, carbon and nitrogen content in the tested materials grew with the increasing concentration of APTES modifier, and the largest amount of the analyzed elements was found for photocatalysts modified with the 650 mM of APTES. However, the highest growth was observed when the concentration increased from 50 to 250 mM. Further increase contributed to slight growth in the amount of the tested elements. Moreover, the data derived from the FT-IR/DR spectra (Fig. 2A–D) agreed with the carbon and nitrogen elemental analysis, which showed a continued increase of C and N in APTES/TiO_2 nanomaterials as the amount of modifier increases. Additionally, at constant APTES concentration, no significant effect of the modification temperature in the range of 120°C to 180°C on carbon and nitrogen contents in the tested materials was found. The presence of 0.18 wt.% nitrogen in the starting-TiO_2 can be explained by the preparation procedure, involving preliminary rinsing with ammonia water, applied to remove residual sulfuric acid from the raw TiO_2 slurry prepared by sulfate technology.

3.1.6. SEM images and EDX mapping

Following the SEM images of the starting-TiO_2 and TiO_2-4h-180°C-650mM sample exhibited in Fig. 3A and B, respectively, it was observed that on the surface of the starting-TiO_2, the grains formed small uniformly distributed aggregates. After TiO_2 functionalization with APTES (Fig. 3B), it was noted that modification increased the size of the aggregates. However, the nanomaterial particles were still characterized by irregular and unspecified shapes. Based on the results of EDX mapping analysis, along with the element stratification and the distribution diagram of an appropriate examined element shown in Fig. 3C and D, it was found that the tested nanomaterials contained Ti, O, C, N and Si elements. Furthermore, it was noted that all elements were homogeneously dispersed over the entire surface of the photocatalyst. The data presented in Table 3 shows that the Si content tends to increase with increasing concentration of the used modifier. Hence, the highest Si content was observed for photocatalyst modified with the APTES concentration of 650 mM.

3.2. Optimization of antibacterial studies

In the first stage of the study, the optimum concentration of photocatalyst for bacteria inactivation in water was determined. Optimization of photocatalyst concentration

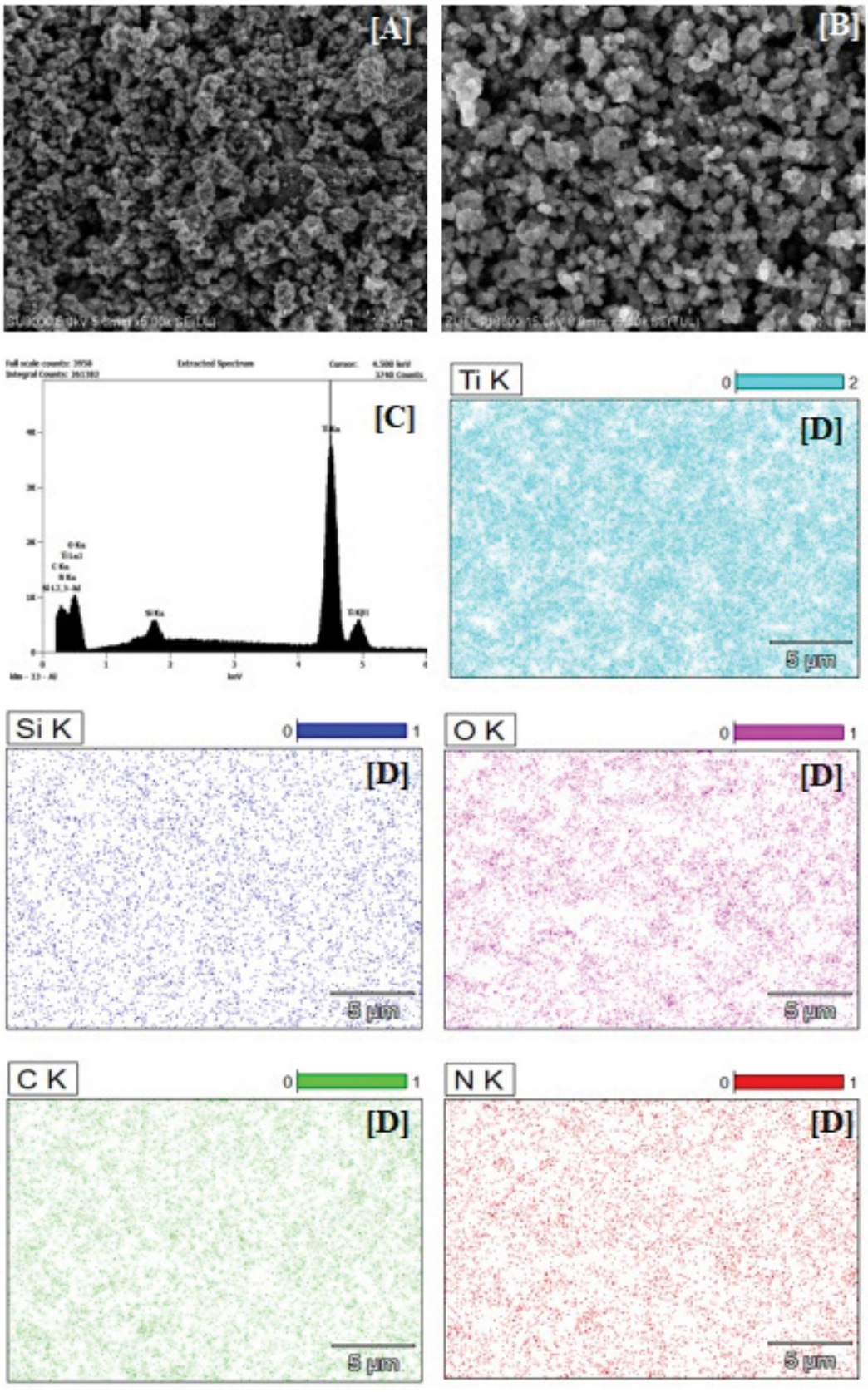

Fig. 3. Example SEM images of starting-TiO_2 (A), and TiO_2-4h-180°C-650mM (B), EDX spectrum (C) and EDX mappings of TiO_2-4h-180°C-650mM (D).

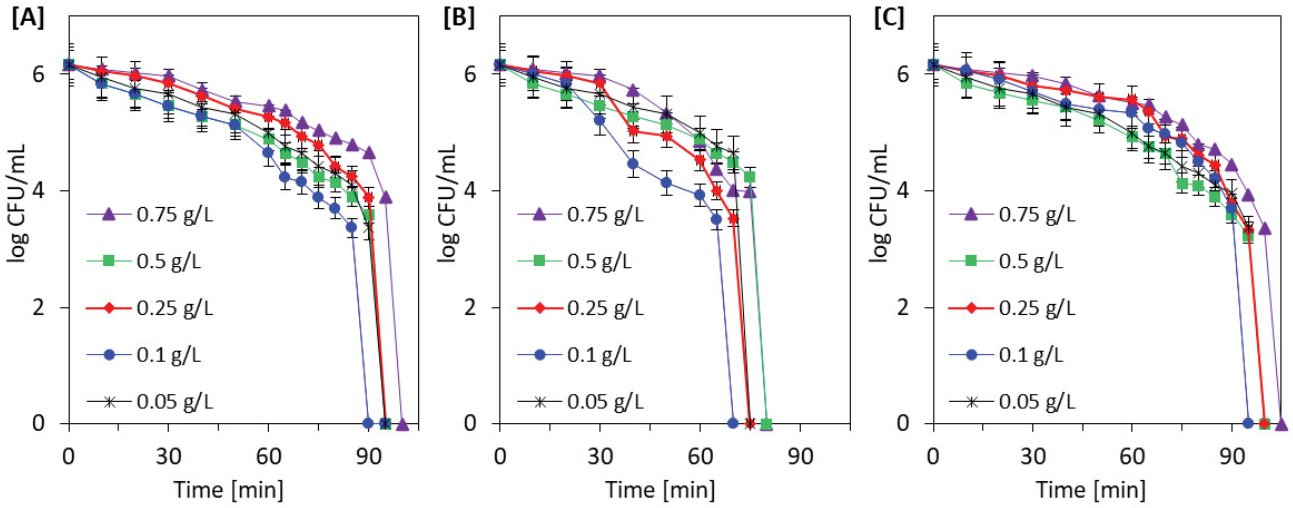

Fig. 4. Inactivation of *E. coli* in the presence of various concentrations of starting-TiO_2 (A), TiO_2-4h-120°C-250mM (B) and TiO_2-4h-160°C-650mM (C) under UV irradiation.

was performed using 3 randomly selected photocatalysts (starting-TiO_2, TiO_2-4h-120°C-250mM and TiO_2-4h-160°C-650 mM) in five concentration (0.05, 0.1, 0.25, 0.5 or 0.75 g/L). In turn, the initial *E. coli* concentration in the reaction mixture amounted approx. 1.5 × 10^6 CFU/mL, according to our previous studies [21,43], was an optimal concentration of bacteria. The fastest bacteria inactivation was observed for all examined samples for a photocatalyst dose of 0.1 g/L (Fig. 4A–C). Therefore, a concentration of 0.1 g/L has been selected as the optimal dose for photocatalytic antibacterial tests. It was also observed that both an increase and a decrease in photocatalysts dose caused extension of time needed for total bacteria inactivation. The dose of 0.05 g/L could be insufficient. In turn, at higher photocatalyst concentration, the activation of TiO_2 particles may be hindered. The increased turbidity of the suspension caused a screening effect and impeded radiation access [44].

A control experiment in the darkness showed that the bacterial number remained unchanged after 90 min of incubation (Fig. S2A–D). Thus, this indicated no toxic effect of the APTES/TiO_2 samples to *E. coli*. Furthermore, the influence of the photolysis on bacterial cells under UV irradiation was also not found (results for NaCl solution presented in Fig. 5A–D).

The bacteria inactivation was observed only in experiments conducted in the presence of APTES/TiO_2 under UV irradiation. As was presented in Fig. 5A–D, APTES/TiO_2 presented better antibacterial properties than starting-TiO_2. The better antibacterial activity was presented for photocatalysts obtained by modification with a 250 mM modifier solution. For this group of photocatalysts, 100% of bacteria were inactivated after 65 min UV irradiation.

Studies have shown that the antibacterial properties strongly depended on the amount of APTES in a solution used for modification and the amount of silica (confirmed by EDX analysis see Table 3), carbon and nitrogen in samples. This, in turn, contributes to changes in the zeta potential of APTES/TiO_2 samples. As shown in Table 2, the zeta potential value increased with increasing carbon and nitrogen content from +12.80 mV for starting-TiO_2 to +27.11 mV for TiO_2-4h-160°C-650 mM, respectively. Therefore, the positively charged surface of APTES/TiO_2 presented a higher potential of contact with the negatively charged *E. coli* cells (−44.2 mV), which led to faster bacteria inactivation. However, the group of samples presented the better antimicrobial properties (TiO_2-4h-120°C-250 mM – TiO_2-4h-180°C-250 mM) were characterized by the less positive zeta potential (from +17.89 to +22.34 mV) in comparison to samples modified by 450 (from +23.12 to +26.73 mV) or 650 mM (from +24.90 to +27.11 mV) of modifier. A similar observation was presented in our previous works [21,43], where this phenomenon was explained by the amount of photogenerated hydroxyl radicals (•OH) produced on nanomaterials surface during the photocatalytic process. It is recognized that •OH radicals play a crucial role in the photocatalytic inactivation of microorganisms, especially bacteria [13,45,46]. In this case, the amount of •OH produced on photocatalysts surface during UV radiation was also examined and obtained results were presented in Fig. 6A–D. The hydroxyl radicals' formation analysis showed that the highest amounts of •OH radicals were observed for a group of samples modified by 250 mM of APTES solution (Fig. 6B). Therefore, a large number of hydroxyl radicals generated during the photocatalytic process led to faster inactivation of *E. coli* in water. Additionally, a two-step mechanism of bacteria destruction in the presence of APTES-modified photocatalyst was observed, which was in accordance with results presented by Desai and Kowshik [47]. As shown from Figs. 4 and 5, the bacteria inactivation proceeded in two phases. In the first phase, the number of live *E. coli* bacteria after the first 80 min of the photocatalytic process was relatively high. Bacteria could trigger some self-repair and self-defence mechanisms [43,47]. In the second stage of the photocatalytic process, many highly reactive radicals led to disturbances and damages in bacteria cells. The cell membranes and walls

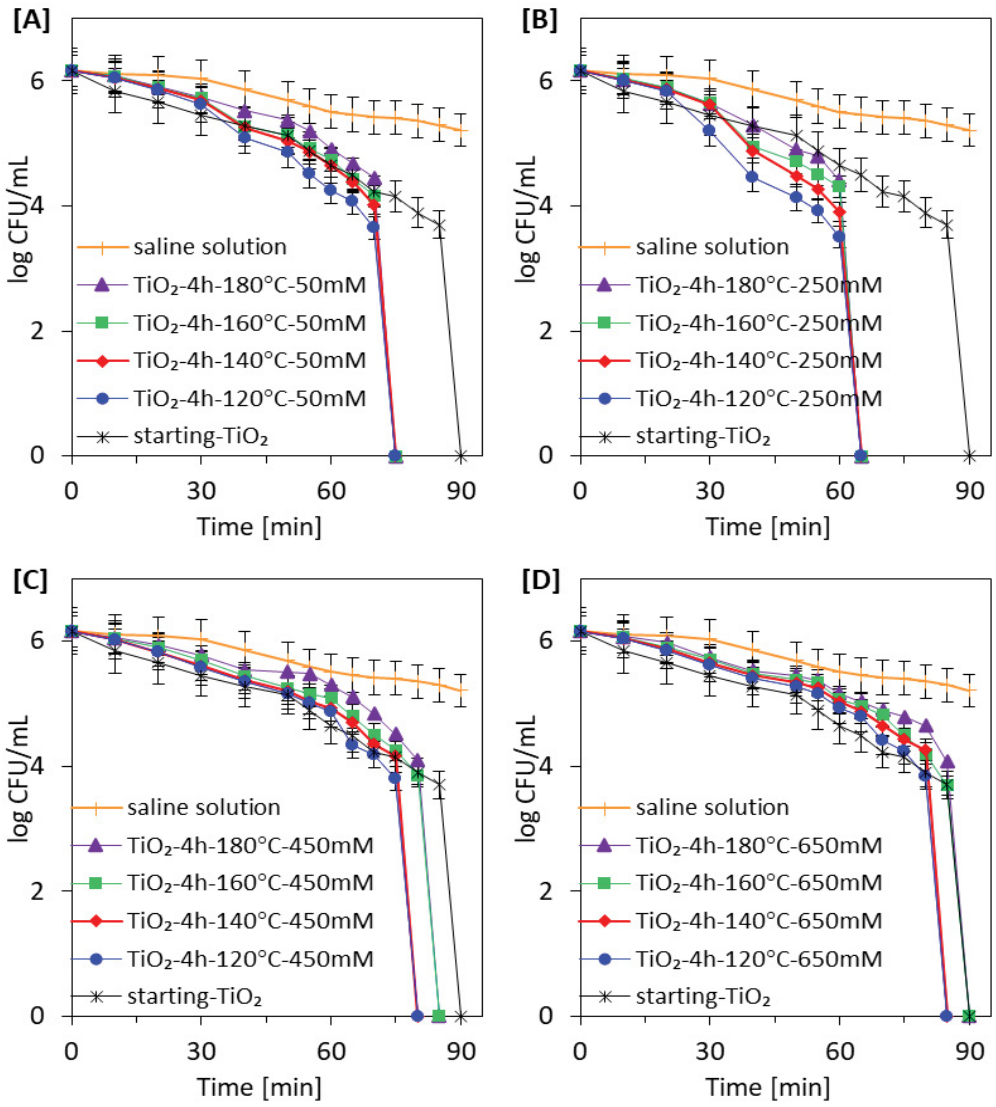

Fig. 5. Inactivation of *E. coli* in the presence of starting-TiO_2 and TiO_2 nanomaterials modified with various APTES concentration: 50 mM (A), 250 mM (B), 450 mM (C), and 650 mM (D) under UV irradiation.

Table 3
Silicon EDX mapping results for APTES/TiO_2 nanomaterials

Element \ Sample name	TiO_2-4h-180°C-50mM	TiO_2-4h-180°C-250mM	TiO_2-4h-180°C-450mM	TiO_2-4h-180°C-650mM
Si (at.%)	0.33	0.74	1.15	1.35

became permeable, and intracellular cytoplasmic components began to leak from the cells. As a consequence, a rapid bacteria inactivation was observed.

It should also be mentioned that increasing the modification temperature from 120°C to 180°C had no significant effect on the antibacterial properties of samples. The temperature did not affect the antimicrobial properties in samples modified with 50 and 250 mM of the modifier solution. In turn, in the case samples modified with 450 and 650 mM of APTES solution at 160°C and 180°C, the time needed to total bacteria inactivation slightly increased (by 5 min) in comparison to lower temperatures of modification.

3.3. Optimization of photocatalytic activity studies

Prior to the photocatalytic activity studies, tests were conducted to investigate the adsorption–desorption equilibrium at the semiconductor-methylene blue

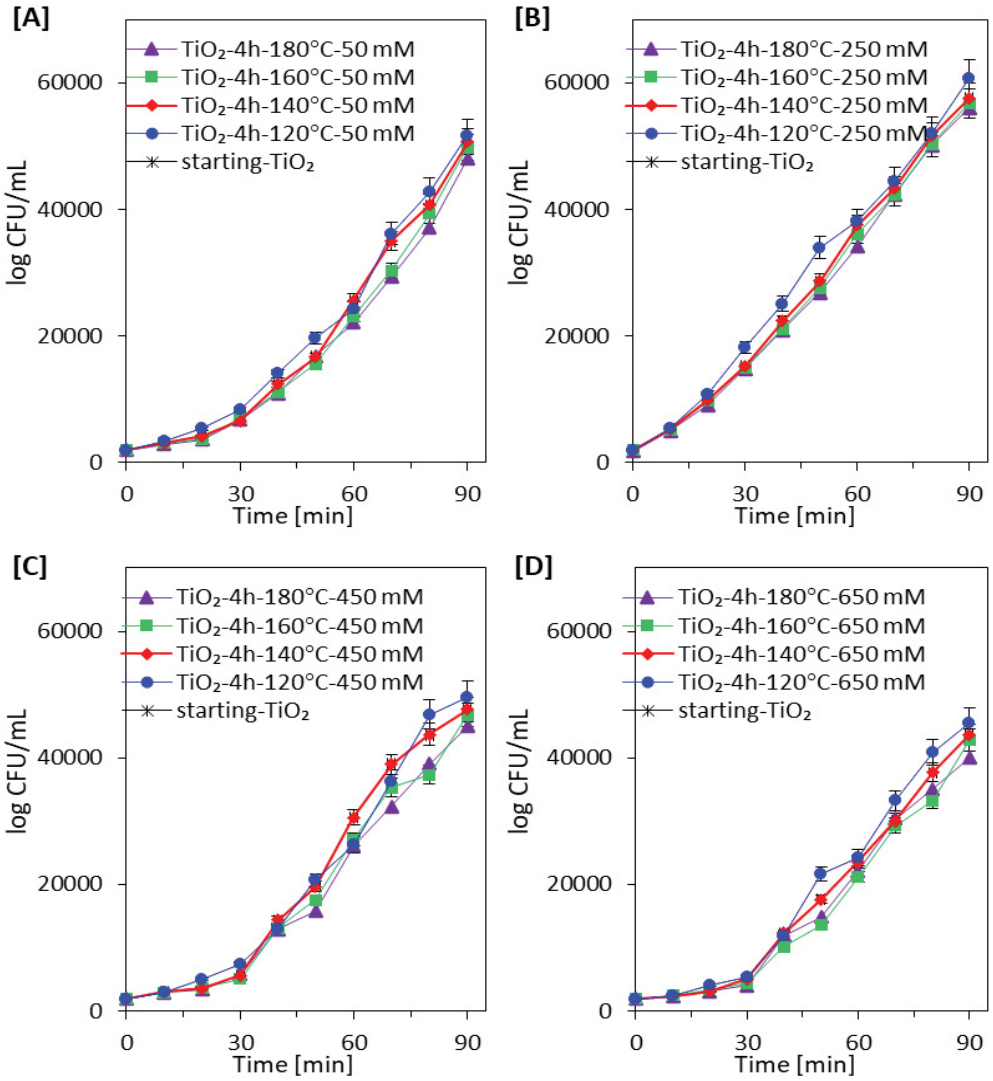

Fig. 6. The amount of generated 2-hydroxyterephthalic acid expressed as the peak area of the fluorescent product during UV irradiation.

interface. Based on the results shown in Figs. S3A–C and S4A–D, it was observed that the dye adsorption degree under light-free conditions was not dependent on either the dose of photocatalyst or the modification temperature or the APTES concentration. For all tested samples, the adsorption–desorption equilibrium was established after 60 min. According to the zeta potential values presented in Table 2, starting-TiO_2 and all APTES-modified TiO_2 nanomaterials exhibited positively charged surfaces. Moreover, it is well known that the positively charged semiconductor surface has a low potential of contact with methylene blue molecules, which is a positively charged cationic dye. Therefore, the adsorption of the dye was negligible, with a maximum of 4% [48–51].

The photocatalytic activity of the starting-TiO_2 and APTES/TiO_2 nanomaterials was evaluated by the methylene blue decomposition under exposure to UV light. To determine the appropriate dose of photocatalyst, three random samples were selected from the entire series of prepared materials and tested for five different concentrations: 0.05, 0.1, 0.25, 0.5 and 0.75 g/L. From the results shown in Fig. 7A–C, it was found that, in general, the photocatalytic activity increased with the increase of the photocatalyst concentration. Although the highest degree of dye decomposition for most samples was observed for 0.75 g/L, a concentration of 0.2 g/L lower, that is, 0.5 g/L, was suitable for further photocatalytic activity tests. For all the materials tested, the difference in the efficiency achieved for the two highest dosages after 360 min of UV irradiation was minor and ranged from 4% to 9%. Considering the slight difference in yield and economic considerations, the less nanomaterial needed, the better, 0.5 g/L was an appropriate sample dosage. Therefore, the photocatalytic activity of all remaining nanomaterials was determined only for the best semiconductor concentration of 0.5 g/L.

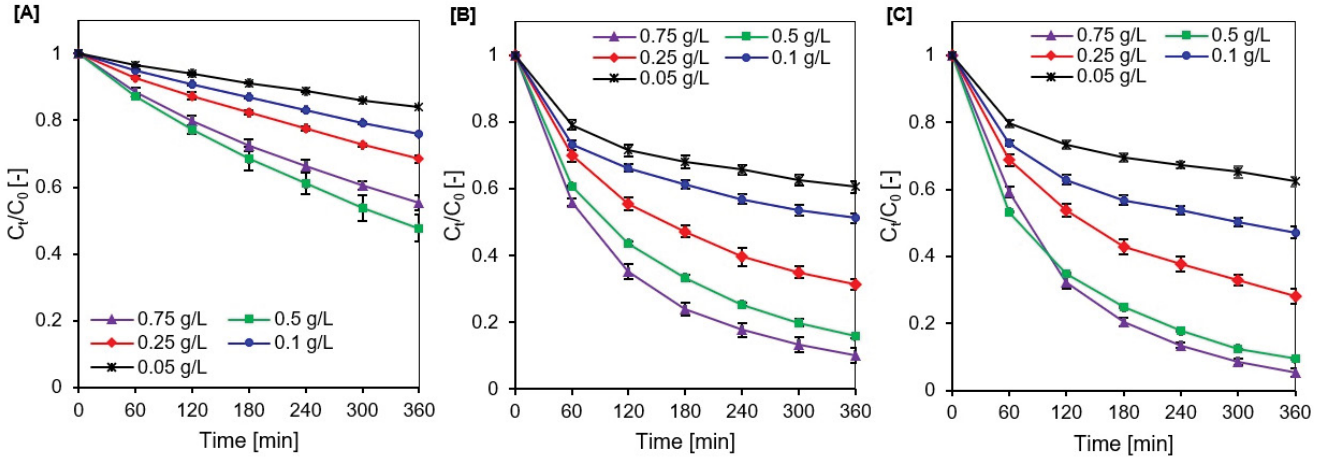

Fig. 7. Methylene blue decomposition under UV irradiation for selected photocatalysts: starting-TiO_2 (A), TiO_2-4h-120°C-250mM (B) and TiO_2-4h-160°C-650mM (C).

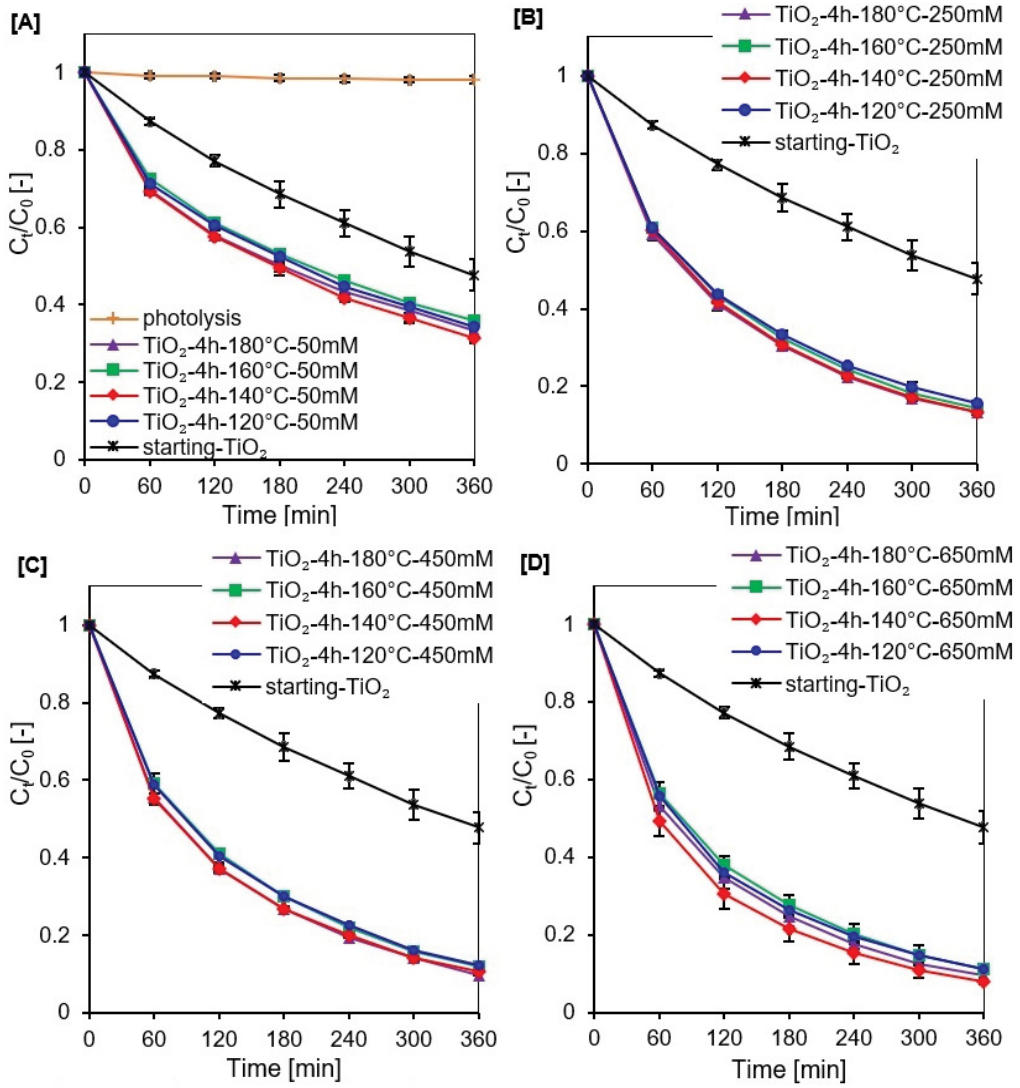

Fig. 8. Methylene blue decomposition under UV irradiation for starting-TiO_2 and APTES/TiO_2 photocatalysts (concentration of semiconductor 0.5 g/L).

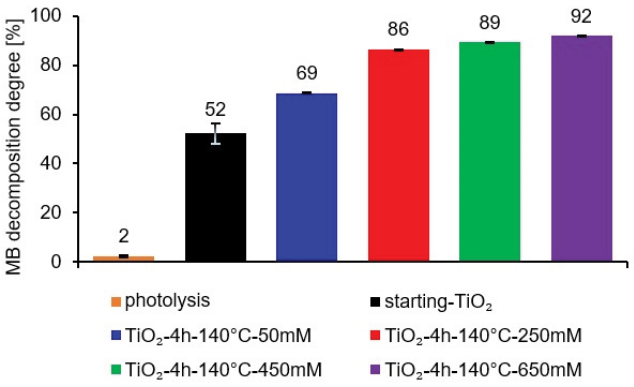

Fig. 9. Methylene blue decomposition degree after 360 min of UV light irradiation for starting-TiO_2 and APTES/TiO_2 photocatalysts (concentration of semiconductor 0.5 g/L).

According to Fig. 8A, tests performed without photocatalyst demonstrated that dye degradation by photolysis was marginal compared to the photocatalysis processes, resulting in about 2% methylene blue degradation after 360 min of exposure same conditions as in the photoactivity measurements. It was noted that all prepared APTES-functionalized TiO_2 samples exhibited a higher dye decomposition degree than starting-TiO_2. Furthermore, the amount of utilized modifier influenced the photocatalytic performance significantly. It was observed that the photoactivity increased with the increasing concentration of APTES used for modification. The highest decomposition degree of about 92% was noted for materials modified with 650 mM modifier solution, while it was only 52% for starting-TiO_2 (Fig. 9). Our observations were consistent with the results obtained by Kassir et al. [52], who also noted that the higher the amount of organosilane used for modification, the better the efficiency of the pollutants decomposition process. Based on the silicon EDX mapping results for APTES/TiO_2 samples (Table 3) and the carbon and nitrogen content analysis (Table 2), it can be concluded that the enhancement of photoactivity with the increase of APTES concentration can be related to the increase of Si, N and C content in the prepared nanomaterials. According to Bui et al. [53], the effect of Si modification on the photoactivity can be attributed to the easy transfer and separation of photogenerated holes and electrons. Also, Viet et al. [54] observed that the performance of silicon-modified TiO_2 was enhanced by adding increasing numbers of Si atoms in the crystal structure. In contrast, Zamiri et al. [55] observed that an increase in the amount of C and N in the modified TiO_2 particles will enhance the number of absorbed photons, resulting in improved degradation efficiency of pollutants. Moreover, it was also noted that increasing the modification temperature from 120°C to 180°C had no significant influence on the activity of the tested samples (Fig. 8A–D).

Summarizing, it was generally concluded that the temperature of modification in the range from 120°C to 180°C was too low to significantly affect the photocatalytic inactivation of bacteria *E. coli* and the efficiency of the methylene decomposition. In contrast, the APTES concentration used for a modification had a key influence on the efficiency of the obtained nanomaterials.

4. Conclusions

The APTES-modified TiO_2 nanomaterials were obtained via solvothermal process at 120°C, 140°C, 160°C and 180°C with the concentrations of APTES equal 50, 250, 450, or 650 mM. The studies confirmed the presence of C, N and Si in the TiO_2 structure, indicating that the modification was carried out successfully. It was noted that APTES inserts into both the external surface of the semiconductor and the pores, resulting in reduced S_{BET} values and pore volumes. It was found that for photocatalytic inactivation of bacteria *E. coli* studies, the best concentration of the photocatalyst was 0.1 g/L, while for methylene blue degradation tests, the best dose of the sample was 0.5 g/L. It was generally observed that all APTES/TiO_2 nanomaterials exhibited higher activity than starting-TiO_2. The best antibacterial properties were observed for a group of samples modified by 250 mM of APTES, attributed to the highest amount of $^{\bullet}OH$ radicals generated from the surface and positive zeta potential (from +17.89 to +22.34 mV). In the case of methylene blue decomposition, the photoactivity increased with increasing concentration of APTES used for modification which can be related to the growth of Si, N and C content in the nanomaterials. After 360 min of UV irradiation, the highest methylene blue decomposition degree was noted for samples modified with 650 mM of APTES. The temperature of modification in the range from 120°C to 180°C had no significant effect on antibacterial properties and the efficiency of the dye decomposition.

Acknowledgement

This work was supported by grant 2017/27/B/ST8/02007 from the National Science Centre, Poland.

Conflicts of interest

The corresponding author states no conflict of interest on behalf of all authors.

References

[1] A.Y. Hoekstra, J. Buurman, K.C.H. van Ginkel, Urban water security: a review, Environ. Res. Lett., 13 (2018) 053002, doi: 10.1088/1748-9326/aaba52.
[2] N. Allocati, M. Masulli, M.F. Alexeyev, C. Di Ilio, *Escherichia coli* in Europe: an overview, Int. J. Environ. Res. Public Health, 10 (2013) 6235–6254.
[3] S. Zhang, M. Abbas, M.U. Rehman, Y. Huang, R. Zhou, S. Gong, H. Yang, S. Chen, M. Wang, A. Cheng, Dissemination of antimicrobial resistance genes (ARGs) via integrons in *Escherichia coli*: a risk to human health, Environ. Pollut., 266 (2020) 115260, doi: 10.1016/j.envpol.2020.115260.
[4] M. Ismail, K. Akhtar, M.I. Khan, T. Kamal, M.A. Khan, A. Asiri, J. Seo, S.B. Khan, Pollution, toxicity and carcinogenicity of organic dyes and their catalytic bio-remediation, Curr. Pharm. Des., 25 (2019) 3645–3663.
[5] A. Tkaczyk, K. Mitrowska, A. Posyniak, Synthetic organic dyes as contaminants of the aquatic environment and their implications for ecosystems: a review, Sci. Total Environ., 717 (2020) 137222, doi: 10.1016/j.scitotenv.2020.137222.

[6] R.A. Capeli, T. Belmonte, J. Caierão, C.J. Dalmaschio, S.R. Teixeira, V.R. Mastelaro, A.J. Chiquito, M.D. Teodoro, J.F.M. Domenegueti, E. Longo, L.G. Trindade, F.M. Pontes, Effect of hydrothermal temperature on the antibacterial and photocatalytic activity of WO_3 decorated with silver nanoparticles. J. Sol-Gel Sci. Technol., 97 (2021) 228–244.
[7] C. El Bekkali, J. Labrag, A. Oulguidoum, I. Chamkhi, A. Laghzizil, J.-M. Nunzi, D. Robert, J. Aurag, Porous ZnO/hydroxyapatite nanomaterials with effective photocatalytic and antibacterial activities for the degradation of antibiotics, Nanotechnol. Environ. Eng., 7 (2022) 1–9, doi: 10.1007/s41204-021-00172-7.
[8] G. Gnanamoorthy, V.K. Yadav, K.K. Yadav, K. Ramar, J. Alam, A.K. Shukla, F.A. Ahmed Ali, M. Alhoshan, Fabrication of different SnO_2 nanorods for enhanced photocatalytic degradation and antibacterial activity, Environ. Sci. Pollut. Res., (2021) 1–11, doi: 10.1007/s11356-021-13627-w.
[9] R. Sharma, Uma, S. Singh, A. Verma, M. Khanuja, Visible light induced bactericidal and photocatalytic activity of hydrothermally synthesized $BiVO_4$ nano-octahedrals, J. Photochem. Photobiol., B, 162 (2016) 266–272.
[10] H.A. Foster, I.B. Ditta, S. Varghese, A. Steele, Photocatalytic disinfection using titanium dioxide: spectrum and mechanism of antimicrobial activity, Appl. Microbiol. Biotechnol., 90 (2011) 1847–1868.
[11] C.S. Uyguner Demirel, N.C. Birben, M. Bekbolet, A comprehensive review on the use of second generation TiO_2 photocatalysts: microorganism inactivation, Chemosphere, 211 (2018) 420–448.
[12] A.O. Ibhadon, P. Fitzpatrick, Heterogeneous photocatalysis: recent advances and applications, Catalysts, 3 (2013) 189–218.
[13] P. Venkata Laxma Reddy, B. Kavitha, P.A.K. Reddy, K.-H. Kim, TiO_2-based photocatalytic disinfection of microbes in aqueous media: a review, Environ. Res., 154 (2017) 296–303.
[14] H.M. Yadav, J.-S. Kim, S.H. Pawar, Developments in photocatalytic antibacterial activity of nano TiO_2: a review, Korean J. Chem. Eng., 33 (2016) 1989–1998.
[15] M.R. Al-Mamun, S. Kader, M.S. Islam, M.Z.H. Khan, Photocatalytic activity improvement and application of UV-TiO_2 photocatalysis in textile wastewater treatment: a review, J. Environ. Chem. Eng., 7 (2019) 103248, doi: 10.1016/j.jece.2019.103248.
[16] R. Li, T. Li, Q. Zhou, Impact of titanium dioxide (TiO_2) modification on its application to pollution treatment—a review, Catalysts, 10 (2020) 804, doi: 10.3390/catal10070804.
[17] R. Klaysri, T. Tubchareon, P. Praserthdam, One-step synthesis of amine-functionalized TiO_2 surface for photocatalytic decolorization under visible light irradiation, J. Ind. Eng. Chem., 45 (2017) 229–236.
[18] G. Xu, Z. Zheng, Y. Wu, N. Feng, Effect of silica on the microstructure and photocatalytic properties of titania, Ceram. Int., 35 (2009) 1–5.
[19] D.M. Tobaldi, A. Tucci, A.S. Škapin, L. Esposito, Effects of SiO_2 addition on TiO_2 crystal structure and photocatalytic activity, J. Eur. Ceram., 30 (2010) 2481–2490.
[20] A. Sienkiewicz, A. Wanag, E. Kusiak-Nejman, E. Ekiert, P. Rokicka-Konieczna, A.W. Morawski, Effect of calcination on the photocatalytic activity and stability of TiO_2 photocatalysts modified with APTES, J. Environ. Chem. Eng., 9 (2021) 104794, doi: 10.1016/j.jece.2020.104794.
[21] P. Rokicka-Konieczna, A. Wanag, A. Sienkiewicz, E. Kusiak-Nejman, A.W. Morawski, Antibacterial effect of TiO_2 nanoparticles modified with APTES, Catal. Commun., 134 (2020) 105862, doi: 10.1016/j.catcom.2019.105862.
[22] A. Wanag, A. Sienkiewicz, P. Rokicka-Konieczna, E. Kusiak-Nejman, A.W. Morawski, Influence of modification of titanium dioxide by silane coupling agents on the photocatalytic activity and stability, J. Environ. Chem. Eng., 8 (2020) 103917, doi: 10.1016/j.jece.2020.103917.
[23] C. Byrne, R. Fagan, S. Hinder, D.E. McCormack, S.C. Pillai, New approach of modifying the anatase to rutile transition temperature in TiO_2 photocatalysts, RSC Adv., 6 (2016) 95232, doi: 10.1039/C6RA19759K.
[24] P. Praveen, G. Viruthagiri, S. Mugundan, N. Shanmugam, Structural, optical and morphological analyses of pristine titanium di-oxide nanoparticles – synthesized via sol-gel route, Spectrochim. Acta, Part A, 117 (2014) 622–629.
[25] M. Ghosh, M. Mondal, S. Mandal, A. Roy, S. Chakrabarty, G. Chakrabarti, S.K. Pradhan, Enhanced photocatalytic and antibacterial activities of mechanosynthesized TiO_2–Ag nanocomposite in wastewater treatment, J. Mol. Struct., 1211 (2020) 1280762, doi: 10.1016/j.molstruc.2020.128076.
[26] A. Razmjou, J. Mansouri, V. Chen, The effects of mechanical and chemical modification of TiO_2 nanoparticles on the surface chemistry, structure and fouling performance of PES ultrafiltration membranes, J. Membr. Sci., 378 (2011) 73–84.
[27] D. Meroni, L. Lo Presti, G. Di Liberto, M. Ceotto, R.G. Acres, K.C. Prince, R. Bellani, G. Soliveri, S. Ardizzone, A close look at the structure of the TiO_2 APTES interface in hybrid nanomaterials and its degradation pathway: an experimental and theoretical study, J. Phys. Chem. C, 121 (2017) 430–440.
[28] A.R.M. Dalod, L. Henriksen, T. Grande, M.-A. Einarsrud, Functionalized TiO_2 nanoparticles by single-step hydrothermal synthesis: the role of the silane coupling agents, Beilstein J. Nanotechnol., 8 (2017) 304–312.
[29] V.A. Zeitler, C.A. Brown, The infrared spectra of some Ti–O–Si, Ti–O–Ti and Si–O–Si compounds, J. Phys. Chem., 61 (1957) 1174–1177.
[30] Q. Chen, N.L. Yakovlev, Adsorption and interaction of organosilanes on TiO_2 nanoparticles, Appl. Surf. Sci., 257 (2010) 1395–1400.
[31] F. Cheng, S.M. Sajedin, S.M. Kelly, A.F. Lee, A. Kornherr, UV-stable paper coated with APTES-modified P25 TiO_2 nanoparticles, Carbohydr. Polym., 114 (2016) 246–252.
[32] E. Ukaji, T. Furusawa, M. Sato, N. Suzuki, The effect of surface modification with silane coupling agent on suppressing the photo-catalytic activity of fine TiO_2 particles as inorganic UV filter, Appl. Surf. Sci., 254 (2007) 563–569.
[33] A.N. Murashkevich, A.S. Lavitskaya, T.I. Barannikova, I.M. Zharskii, Infrared absorption spectra and structure of TiO_2-SiO_2 composites, J. Appl. Spectrosc., 75 (2008) 730, doi: 10.1007/s10812-008-9097-3.
[34] M. Muttakin, S. Mitra, K. Thu, K. Ito, B.B. Saha, Theoretical framework to evaluate minimum desorption temperature for IUPAC classified adsorption isotherms, Int. J. Heat Mass Transfer, 122 (2018) 795–805.
[35] V.V. Kutarov, E. Robens, Yu. I. Tarasevich, E.V. Aksenenko, Adsorption hysteresis at low relative pressures, Theor. Exp. Chem., 47 (2011) 163–168.
[36] Z. Al-Othman, A review: fundamental aspects of silicate mesoporous materials, Materials, 5 (2012) 2874–2902.
[37] N.R.C. Fernandes Machado, V.S. Santana, Influence of thermal treatment on the structure and photocatalytic activity of TiO_2 P25, Catal. Today, 107–108 (2005) 595–601.
[38] W. Zhuang, Y. Zhang, L. He, R. An, B. Li, H. Ying, J. Wu, Y. Chen, J. Zhou, X. Lu, Facile synthesis of amino-functionalized mesoporous TiO_2 microparticles for adenosine deaminase immobilization, Microporous Mesoporous Mater., 239 (2017) 158–166.
[39] P.I. Pontón, J.R.M. d'Almeida, B.A. Marinkovic, S.M. Savić, L. Mancic, N.A. Rey, E. Morgado, F.C. Rizzo, The effects of the chemical composition of titanate nanotubes and solvent type on 3-aminopropyltriethoxysilane grafting efficiency, Appl. Surf. Sci., 301 (2014) 315–322.
[40] W.A. Talavera-Pech, A. Esparza-Ruiz, P. Quintana-Owen, A.F. Vilchis-Nestor, C. Carrera-Figueiras, A. Ávila-Ortega, Effects of different amounts of APTES on physicochemical and structural properties of amino-functionalized MCM-41-MSNs, J. Sol-Gel Sci. Technol., 80 (2016) 697–708.
[41] Z. Youssef, V. Jouan-Hureaux, L. Colombeau, P. Arnoux, A. Moussaron, F. Baros, J. Toufaily, T. Harmieh, T. Roques-Carmes, C. Frochot, Titania and silica nanoparticles coupled to Chlorin e6 for anti-cancer photodynamic therapy, Photodiagn. Photodyn. Ther., 22 (2018) 115–126.
[42] J. Zhao, M. Milanova, M.M.C.G. Warmoeskerken, V. Dutschk, Surface modification of TiO_2 nanoparticles with silane coupling agents, Colloids Surf., A, 413 (2012) 273–279.

[43] P. Rokicka-Konieczna, A. Wanag, A. Sienkiewicz, E. Kusiak-Nejman, A.W. Morawski, Effect of APTES modified TiO_2 on antioxidant enzymes activity secreted by *Escherichia coli* and *Staphylococcus epidermidis*, Biochem. Biophys. Res. Commun., 534 (2021) 1064–1068.
[44] A.K. Benabbou, Z. Derriche, C. Felix, P. Lejeune, P. Guillard, Photocatalytic inactivation of *Escherischia coli*: effect of concentration of TiO_2 and microorganism, nature, and intensity of UV irradiation, Appl. Catal., B, 76 (2007) 257–263
[45] M. Cho, H. Chung, W. Choi, J. Yoon, Linear correlation between inactivation of *E. coli* and OH radical concentration in TiO_2 photocatalytic disinfection, Water Res., 38 (2004) 1069–1077.
[46] O.K. Dalrymple, E. Stefanakos, M.A. Trotz, D.Y. Goswami, A review of the mechanisms and modeling of photocatalytic disinfection, Appl. Catal., B, 98 (2010) 27–38.
[47] V.S. Desai, M. Kowshik, Antimicrobial activity of titanium dioxide nanoparticles synthesized by sol-gel technique, Res. J. Microbiol., 4 (2009) 97–103.
[48] K. Bubacz, B. Tryba, A.W. Morawski, The role of adsorption in decomposition of dyes on TiO_2 and N-modified TiO_2 photocatalysts under UV and visible light irradiations, Mater. Res. Bull., 47 (2012) 3697–3703.
[49] M.A. Al-Ghouti, R.S. Al-Absi, Mechanistic understanding of the adsorption and thermodynamic aspects of cationic methylene blue dye onto cellulosic olive stones biomass from wastewater, Sci. Rep., 10 (2020) 15928, doi: 10.1038/s41598-020-72996-3.
[50] V. Saxena, D.K. Aswal, Surface modifications of photoanodes in dye sensitized solar cells: enhanced light harvesting and reduced recombination, Semicond. Sci. Technol., 30 (2015) 064005, doi: 10.1088/0268-1242/30/6/064005.
[51] M.R. Shenoy, S. Ayyasamy, M.V.V. Reddy, G. Kadarkarai, J. Suryakanth, S. Tamilarasan, S. Thangavelu, A.Ch. Jeyaramane, The effect of morphology-dependent surface charges of iron oxide on the visible light photocatalytic degradation of methylene blue dye, J. Mater. Sci.: Mater. Electron., 31 (2020) 17703–17717.
[52] M. Kassir, T. Roques-Carmes, K. Assaker, T. Hamieh, A. Razafitianamaharavo, J. Toufaily, F. Villiéras. Enhanced photocatalytic degradation of salicylic acid in water-ethanol mixtures from titanium dioxide grafted with hexadecyltrichlorosilane, Phys. Procedia, 55 (2014) 403–408.
[53] D.-N. Bui, S.-Z. Kang, X. Li, J. Mu, Effect of Si doping on the photocatalytic activity and photoelectrochemical property of TiO_2 nanoparticles, Catal. Commun., 13 (2011) 14–17.
[54] P. Van Viet, T.H. Huy, S.J. You, L.V. Hieu, C.M. Thi, Hydrothermal synthesis, characterization, and photocatalytic activity of silicon doped TiO_2 nanotubes, Superlattices Microstruct., 123 (2018) 447–455.
[55] M. Zamiri, M. Giahi, Photochemical degradation of an anionic surfactant by TiO_2 nanoparticle doped with C, N in aqueous solution, Russ. J. Phys. Chem., 90 (2016) 2668–2674.

Supplementary information

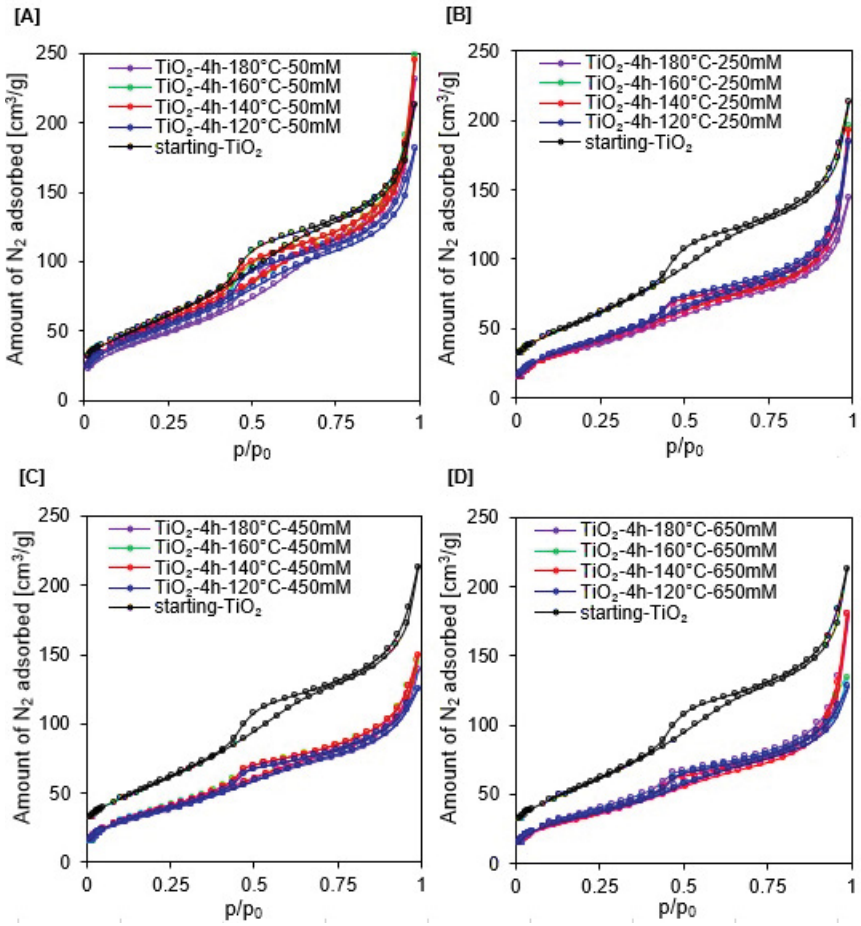

Fig. S1. Adsorption–desorption isotherms of starting-TiO_2 and TiO_2 nanomaterials modified with APTES concentration of 50 mM (A), 250 mM (B), 450 mM (C), and 650 mM (D).

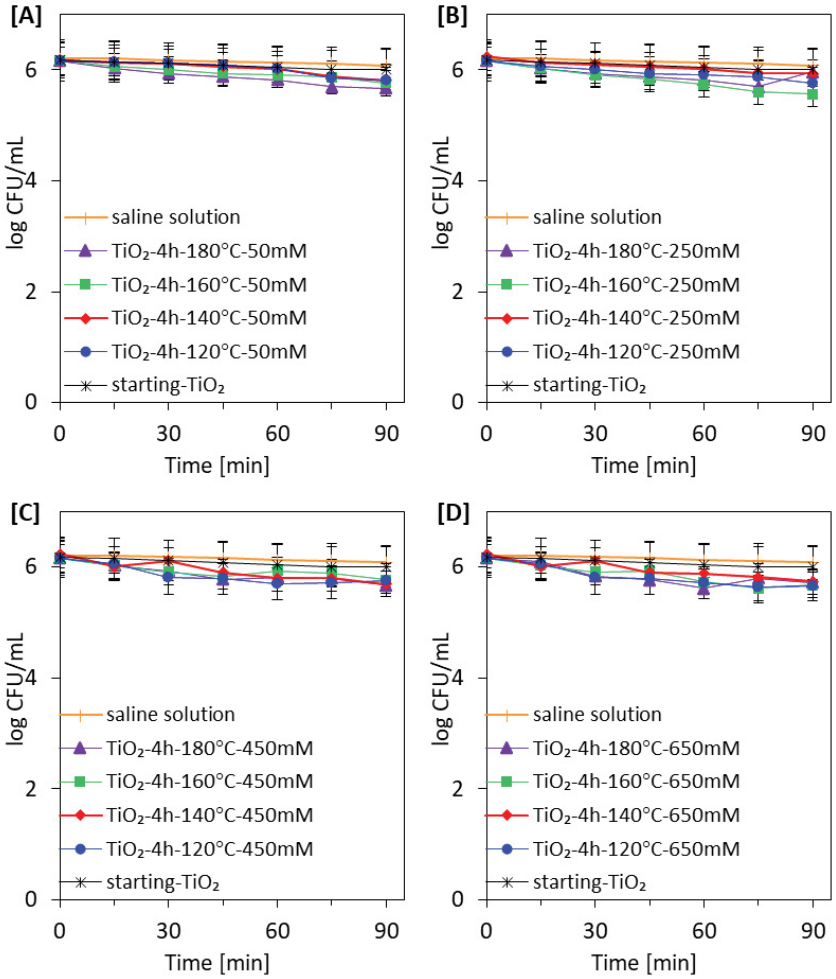

Fig. S2. Inactivation of *E. coli* in the presence of starting-TiO_2 and TiO_2 nanomaterials modified with APTES concentration of 50 mM (A), 250 mM (B), 450 mM (C) and 650 mM (D) under dark conditions.

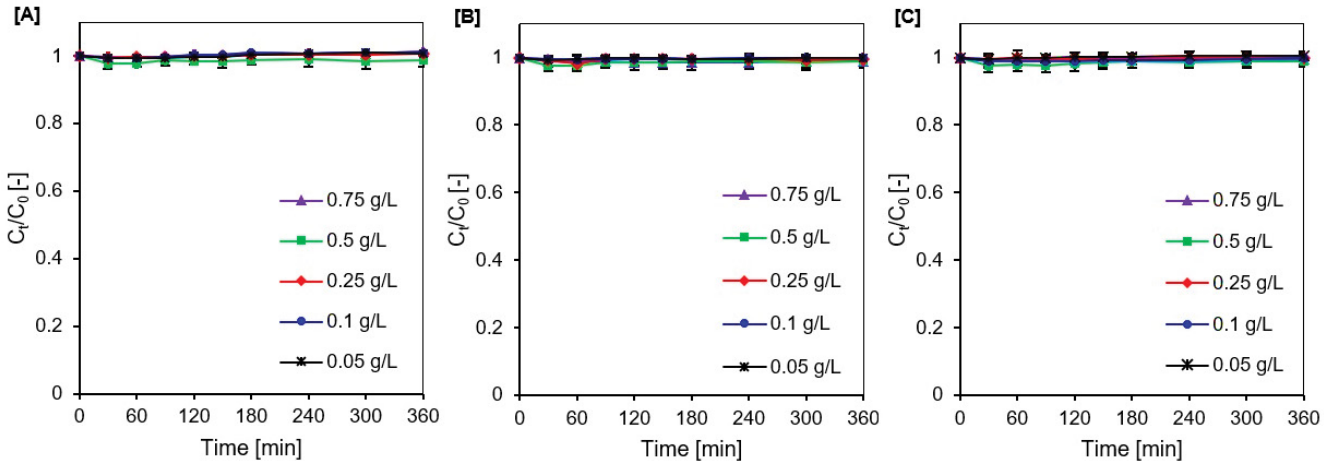

Fig. S3. Methylene blue adsorption degree on the surface of selected photocatalysts: starting-TiO_2 (A), TiO_2-4h-120°C-250mM (B) and TiO_2-4h-160°C-650mM (C).

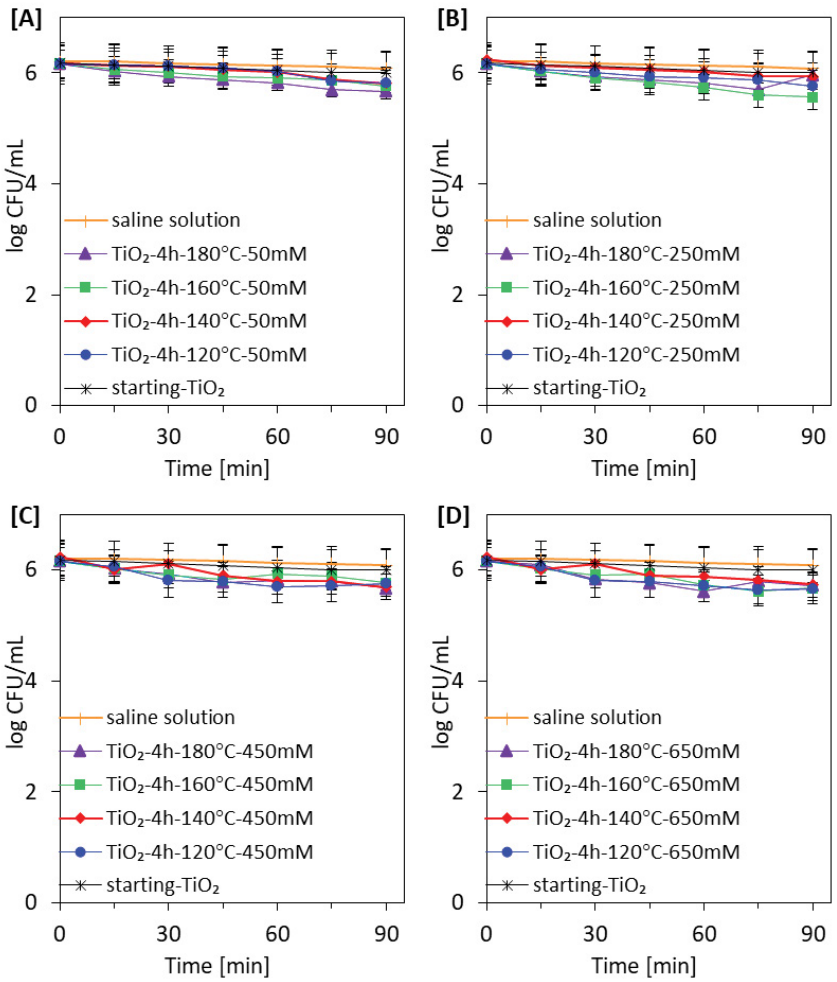

Fig. S4. Methylene blue adsorption degree on the surface of starting-TiO_2 and APTES/TiO_2 photocatalysts (concentration of semiconductor 0.5 g/L)